Materials Science and Engineering A 404 (2005) 49–56

www.elsevier.com/locate/msea

Crystallization behavior of spray-formed and melt-spun $Al_{89}La_6Ni_5$ hybrid composites with amorphous and nanostructured phases

M.L. Ted Guo [a], Chi Y.A. Tsao [a,*], J.C. Huang [b], J.S.C. Jang [c]

[a] *Department of Materials Science and Engineering, National Cheng Kung University, 1 Da-Shieh Rd., 70101 Tainan, Taiwan, ROC*
[b] *Institute of Materials Science and Engineering, National Sun Yat-Sen University, 70 Lien-hai Rd., 804 Kaohsiung, Taiwan, ROC*
[c] *Department of Materials Science and Engineering, I-Shou University, Section 1, Hsueh-Cheng Rd., Ta-Hsu Hsiang, Kaohsiung County 840, Taiwan, ROC*

Received in revised form 11 May 2005; accepted 19 May 2005

Abstract

The crystallization behavior of spray-formed and melt-spun $Al_{89}La_6Ni_5$ alloys was studied. Spray forming process could produce a bulk scale $Al_{89}La_6Ni_5$ hybrid composite consisting of amorphous and nanostructured phases directly without the need of an amorphous precursor. The fraction of amorphous phase in the spray-formed composite was determined to be 36% by DSC, which came mostly from supercooled liquid droplets upon spray forming. Amorphous phase partially devitrified to nano-scale fcc-Al secondary crystals during deposition. Two significant primary crystals observed in the spray-formed bulk hybrid composite are Al_3Ni and $Al_{11}La_3$(Ni), but their size is reduced to about 1 μm. Contrary to the microstructure of spray-formed deposit, the heat-treated and fully devitrified melt-spun ribbon hybrid composite consists of nano-scale fcc-Al, Al_3Ni, $Al_{11}La_3$ as well as some metastable Al_6Ni and Al_4LaNi phases with sizes of about 200 nm. Deformation twins were found in the $Al_{11}La_3$(Ni) crystals in spray-formed deposit, but not in the fully devitrified ribbon. Finally, the microstructure structure evolution of spray-formed deposit and heat-treated ribbon are studied and proposed.

Keywords: Spray forming; Melt spinning; Crystallization; Bulk amorphous; Hybrid nanocomposites

1. Introduction

Since 1988 [1–5], many ultra-high strength (>1 GPa) nanostructured aluminum composites have been developed by proper annealing [6,7] the amorphous Al–RE–TM precursors to precipitate nano Al crystals in the matrix. The uniformly dispersed nano Al crystals retard the movement of shear bands generated in the matrix during deformation and further increase the strength. Thus, the ultra-high strength of the composites are determined by the proper size and distribution combination of nano Al crystals in the matrix, which is significantly different from that of conventional alloys or composites. Generally, the synthesis of nanostructured Al–RE–TM composites needs amorphous phases as precursors. Amorphization of Al–RE–TM alloys require a very large cooling rate, and the melt-spinning technique is by far the most preferred.

Melt-spun ribbons typically have very limited dimensions (2–4 mm in width and 20–50 μm in thickness) and hence many research groups seek to increase the product size. The technique of warm extrusion of amorphous ribbons/or powders was used to form larger bulk samples, but partial crystallization occurred. In this study, spray forming process was employed as a new way to fabricate the nanostructured Al–RE–TM composite.

Spray forming [8–11] is a rapid solidification process in which molten metal is atomized into fine droplets by high-pressure nitrogen gas and then collected into a dense deposit on the substrate after a short flight distance. Its most attractive features are the ability to create refined microstructure and reduced segregation [11,12]. Al–10Ni–5Mm (Misch metal) [13] amorphous sheets (7 mm in thickness and 50 mm in length) have been produced by spray forming process.

* Corresponding author. Tel.: +886 6 2083889; fax: +886 6 2083889.
E-mail address: tsao_cya@alum.mit.edu (C.Y.A. Tsao).

0921-5093/$ – see front matter © 2005 Elsevier B.V. All rights reserved.
doi:10.1016/j.msea.2005.05.088

Lately, spray-formed Al–8Y–5Ni–2Co (2 kg) nanocomposite [14,15] under increased gas/metal ratio (G/M ratio, 10 m^3/kg) resulted in 76% amorphous phase. As G/M ratio decreased to 6.4, the deposit was fully crystallized. Another Al–3Y–8Ni–4Co–1Zr (7 kg) nanocomposite spray formed at somewhat lower G/M ratio (8.7 m^3/kg) was also fully crystallized. These previous studies concluded that the crystallization was due to heat accumulation during deposition. In this study, a liquid nitrogen (LN) cooled Cu substrate was employed to increase the heat dissipation during deposition.

Melt-spun $Al_{89}La_6Ni_5$ ribbons provided both high strength and 180° bending ductility. The glass forming compositions map for Al–La–Ni system was established by Inoue et al. [16], and their study focused on the La-rich corner ($Al_{25}La_{55}Ni_{20}$). The La-based amorphous alloys provided a very beneficial combination of relatively high glass formation ability (low critical cooling rate) and a wide supercooled region (69 K) for glass forming, but these alloys are the most expensive. Al-based (La + Ni < 15 at.%) amorphous alloys can provide significant property improvement with relatively lower glass formation ability and narrow supercooled region at reduced cost.

The selected $Al_{89}La_6Ni_5$ alloy is a hypereutectic alloy and a recent study [17] determined the ternary eutectic composition to be $Al_{95.4}La_{1.7}Ni_{2.9}$. Increasing the solute content to about 10–15% is an empirical rule to further increase glass forming ability. Some previous studies [18,19] also focused on crystallization of $Al_{89}La_6Ni_5$ ribbons under ultra-high pressure, but little information is available on the bulk $Al_{89}La_6Ni_5$ amorphous alloy. In this study, $Al_{89}La_6Ni_5$ was fabricated via the spray forming and melt-spinning processes. The relationship between process parameters and amorphous phase percentage in the resultant deposit (SD) and ribbon (MS30) was investigated. Solidification path, microstructure evolution and primary and secondary crystallizations during spray forming process are also studied.

2. Experimental procedure

An Al–Ni master alloy was prepared by mixing Al (99.8% + Si and Fe) and Al–80Ni flux in N_2 atmosphere, and then remelted it with La (99.9%) under N_2 in a graphite crucible, weighted 5 kg. Molten metal was atomized with N_2 and deposited on a LN-cooled Cu substrate to form a deposit of 230 mm in diameter, 3 mm in thickness and 1 kg in weight. In the case of MS30, molten metal was melt-spun on a Cu wheel with a surface speed of 30 m s^{-1} under Ar to form ribbons of 20–30 μm in thickness and 2–3 mm in width. The spray-formed deposit was designated as SD and melt-spun ribbons as MS30.

The compositions of the alloys were measured by the inductively coupled plasma-mass spectrometry (ICP) method (Perkin-Elmer Optima 3200 RL). The X-ray (Cu Kα) diffraction tests (Rigaku geigerflex) were performed from angles of 20–80° at a scanning speed of 3°/min. Quantitative wavelength diffraction spectrum (WDS) analyses and back-scattered electron imaging (BEI) of the phases were carried out with the WD/ED combined microanalyzer (JEOL™ JXA-8900R). Samples were also investigated by differential scanning calorimeter (DSC) (Perkin-Elmer Pyris1) to determine the reactions during heating. The temperature of the DSC was calibrated within 1 K by the melting temperatures of In and Zn. The heat flow was calibrated by the melting enthalpy of In with an accuracy of 0.1%. Before each measurement, a base line was always established by an empty pan. The structure evolutions of ribbons and deposit were conducted by transmission electron microscopy (TEM) (JEOL AEM3010) equipped with a nano-volume energy dispersive spectrometry (EDS) system. TEM samples were prepared by ion milling (Gatan 691) with angles of 8–4° and with beam energy 4.5 kV and 25 μA.

3. Results and discussions

Fig. 1 shows the XRD diffraction patterns of MS30 heated to various temperatures, and the XRD pattern of SD. The MS30 exhibits typical amorphous halo peak, and the SD shows quite similar pattern with small characteristic peaks of fcc-Al, Al_3Ni, $Al_{11}La_3$ and some unknown phases.

Fig. 2 shows the DSC traces of the MS30 in as-melt-spun condition and in subsequently annealed condition for various times, together with a trace of the SD in as-spray-formed condition. Only the as-melt-spun MS30 exhibits

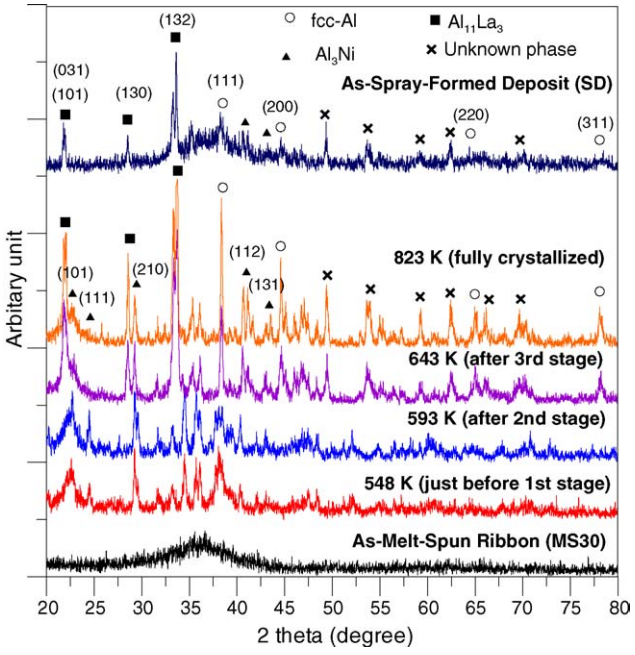

Fig. 1. XRD patterns of the as-melt-spun $Al_{89}La_6Ni_5$ ribbons (MS30) heated in DSC to 548, 593, 643 and 823 K, and XRD patterns of the as-spray-formed $Al_{89}La_6Ni_5$ deposit (SD). Heat rate is 40 K/min.

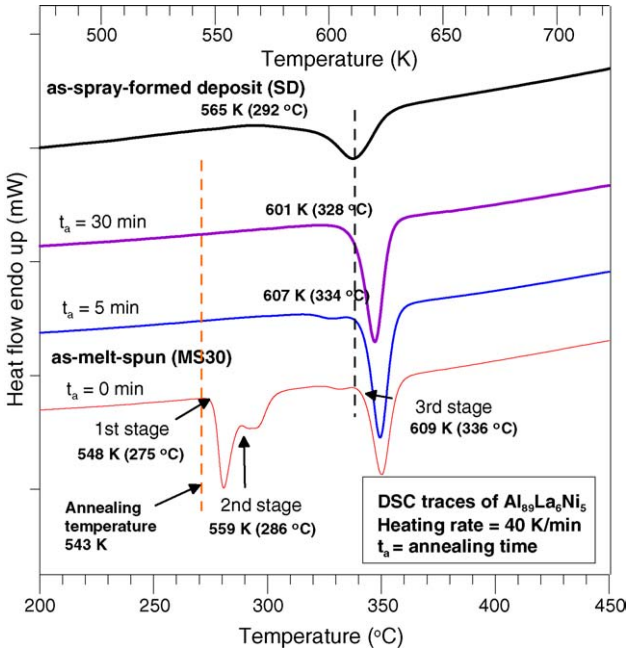

Fig. 2. DSC traces of the $Al_{89}La_6Ni_5$ ribbons (MS30) in as-melt-spun condition and subsequently annealed conditions for various time, together with that of the SD in as-spray-formed condition.

multi-exothermic reactions, which correspond to three devitrification stages with onset temperatures of 548, 593 and 643 K, respectively. The SD shows only the third stage (565 K), suggesting that only a partial amount of amorphous phases exists in it.

To identify the various precipitates in each stage, the MS30 was heated in DSC to various temperatures and examined by XRD, as shown in Fig. 1. As the MS30 was heated, fcc-

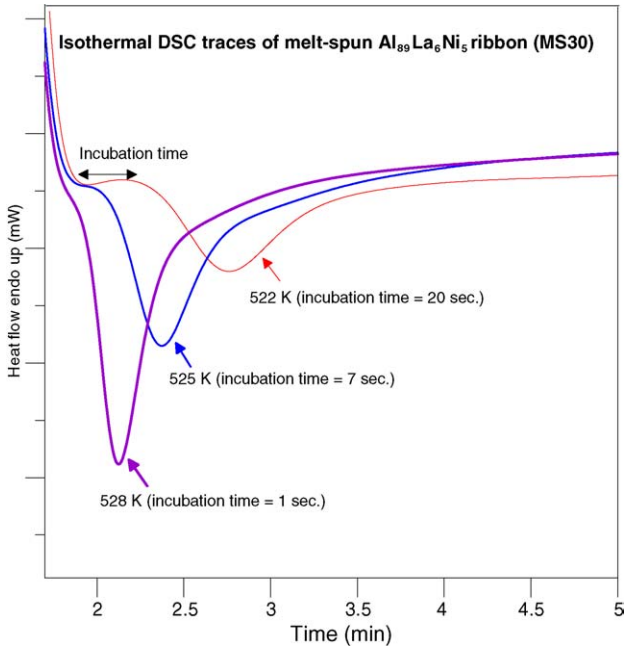

Fig. 3. Isothermal DSC traces of the $Al_{89}La_6Ni_5$ ribbons (MS30) at various temperatures.

Table 1
Enthalpies released during continuously heating the $Al_{89}La_6Ni_5$ alloys (MS30 and SD) in DSC at 40 K/min

kJ/mol	First peak + second peak	Third peak	Total
MS30	60 ± 2	47.5 ± 3	108 ± 3
SD	0	39 ± 2	39 ± 2

Al, Al_3Ni and some unknown metastable crystals occurred just before the first stage (548 K). When heated above the second stage (593 K), the characteristic peaks of Al_3Ni and metastable phases become more significant. When heated over the third stage (643 K), the characteristic peaks of $Al_{11}La_3$ began to appear and the MS30 became fully crystallized. Since then, the MS30 was completely crystallized and the patterns of it remained unchanged until being subsequently heated to 823 K. It should be noted that the XRD pattern of the SD is distinct from that of the MS30 at various stages. Some characteristic peaks of unknown phases in the MS30 were not observed in the SD. In the SD, the halo peak representing amorphous phase co-exists together

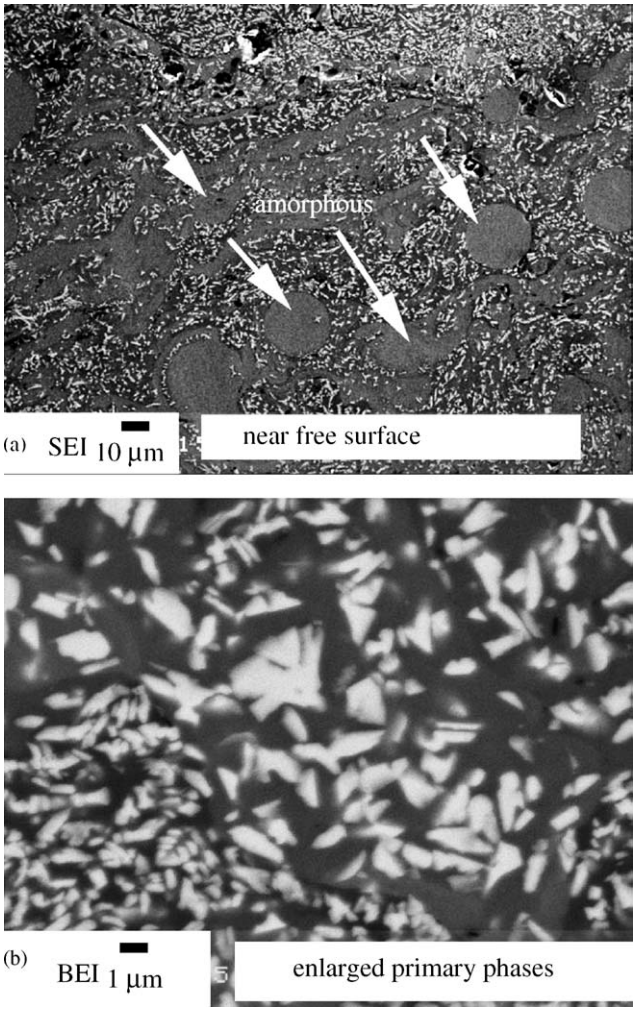

Fig. 4. Micrographs of (a) the as-spray-formed $Al_{89}La_6Ni_5$ deposit near upper surface and (b) the enlarged primary crystals (BEI).

with some characteristic peak, which suggest that the SD is a hybrid composite of amorphous and crystalline phases, and its microstructure is different from that of partial devitrified nanostructured MS30 alloy.

The MS30 ribbons were annealed at 543 K (before the first stage) for various time periods and then rescanned by DSC, as shown in Fig. 2. It was found that as the annealing time increased, the enthalpy of the overlapped first and second peaks, due to precipitation of fcc-Al, Al_3Ni and some unknown phases, disappeared, which indicated that the phases of fcc-Al, Al_3Ni and some unknown phases had precipitated from the amorphous matrix during annealing. The onset temperature of the third stage also reduced as the annealing time increased, which may be due to the fact that the precipitation of the nano-scale crystals during annealing consumed much of the solute (Ni and La elements) in the matrix, resulting in the instability of the retained amorphous matrix, which caused an earlier devitrification reaction. The third stage in the SD trace also occurred much earlier (by 44 K), which because much more solute (Ni and La) was consumed in the amorphous matrix while micro-scale primary crystals were generated during solidification.

Fig. 1 shows that fcc-Al and Al_3Ni phases in the MS30 were present before the first stage (548 K). In order to examine if they were pre-existing phases in the amorphous ribbon, three isothermal DSC tests were performed at 522, 525 and 528 K, as shown in Fig. 3. The results show three typical nucleation and growth curves at all temperatures. After certain incubation time, nucleation occurred in the amorphous matrix and began to grow. The incubation time for nucleation and total reaction time decreased as the heating temperature increased. This trend is similar to the previous results [20–21]. Therefore, fcc-Al and Al_3Ni were not pre-existing phases, and they were formed in the amorphous ribbon by nucleation and growth during heating.

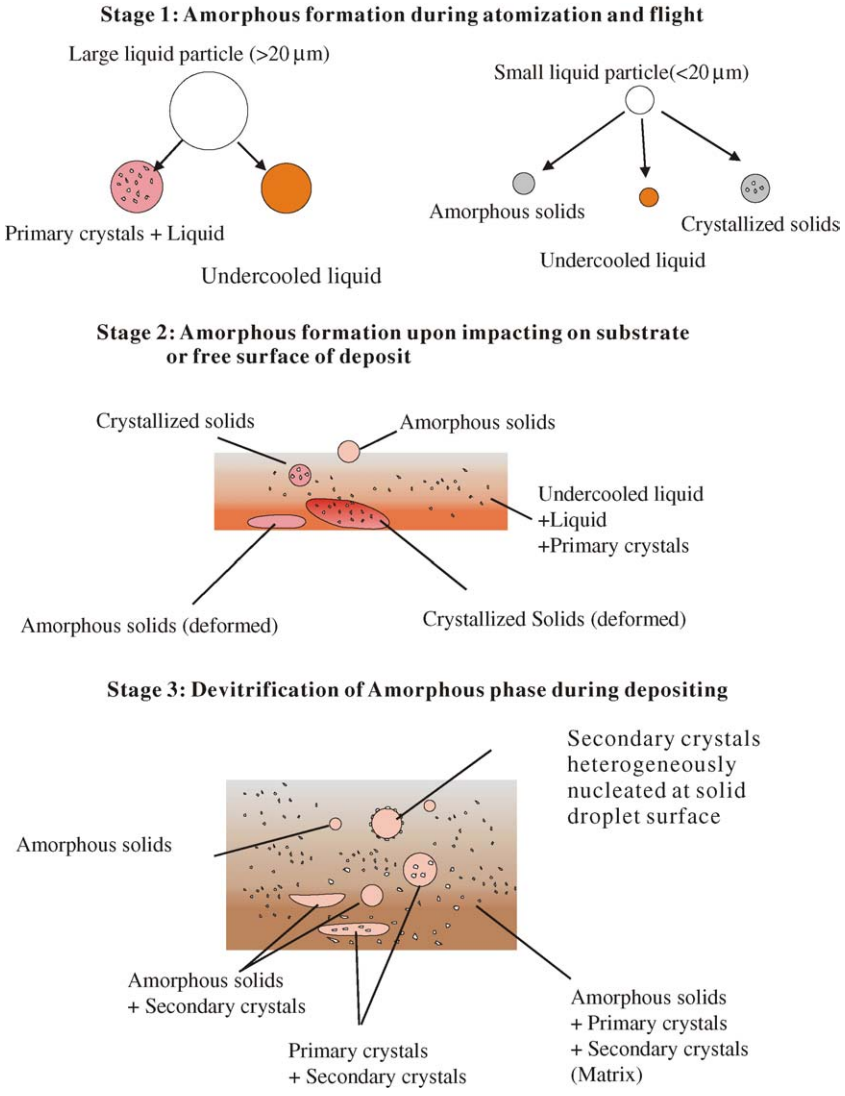

Fig. 5. Schematic sequences of the microstructure evolution during spray forming of hybrid composites.

Table 1 shows the enthalpies released for the SD and MS30 during continuous heating in DSC. The total enthalpy released (from RT to 823 K) from the MS30 is 108 J/g and the total enthalpy released from the SD is 39 J/g. For the convenience of calculation, the MS30 was assumed to be in the fully amorphous state (as the baseline for 100%), even though it contained a small amount of crystalline phases. Therefore, the percentage of amorphous phase of the SD could be determined to be 39/108 = 36% [22,23], while the other 64% correspond to crystalline phases. Since the first + second exothermic peaks of the SD are completely absent during deposition, this also indicates that the corresponding phases have completely precipitated.

Fig. 4 shows the microstructure of the SD. The angular shaped micro-scale primary phases precipitated in the liquid, about 1–2 μm were designated as *primary crystals*, and the nano-scale phases formed during the later solid state reaction as *secondary crystals*. During the spray forming process, undercooled liquid droplets directly impacted the free surface of LN-cooled substrate and subsequently accumulated into a deposit with a thickness of 3 mm. Fig. 4(a) is the secondary electron image (SEI) of the deposit near free surface and Fig. 4(b) is an enlarged back-scattered image (BEI) of localized region of Fig. 4(a). Previous studies [14,15] reported that, in BEI image, amorphous regions exhibited featureless morphology, which were significantly different from the adjacent crystalline region. In this study, the SD shows many featureless regions (arrowed in Fig. 4), which are believed to be amorphous phases, coexisting with other regions full of primary crystals. Fig. 2 also confirms that there is an exothermic peak in the SD, showing that amorphous devitrification did happen during heating in DSC. Therefore, the microstructure of the SD is a hybrid composite consisting of amorphous phases, primary and secondary crystals. Featureless regions can be further divided into two kinds of morphology, irregular layers and near round type. Primary crystals are mostly of sharp angular shape, but some have rod-like shape. From subsequent TEM results (Figs. 6 and 7), the rod-like phase was identified as Al_3Ni and the sharp angular phase as $Al_{11}La_3$. Except for a 10-fold reduction (from 100–200 to 1–2 μm) due to rapid solidification during spray forming, the phases are similar to the primary phases found in a previous

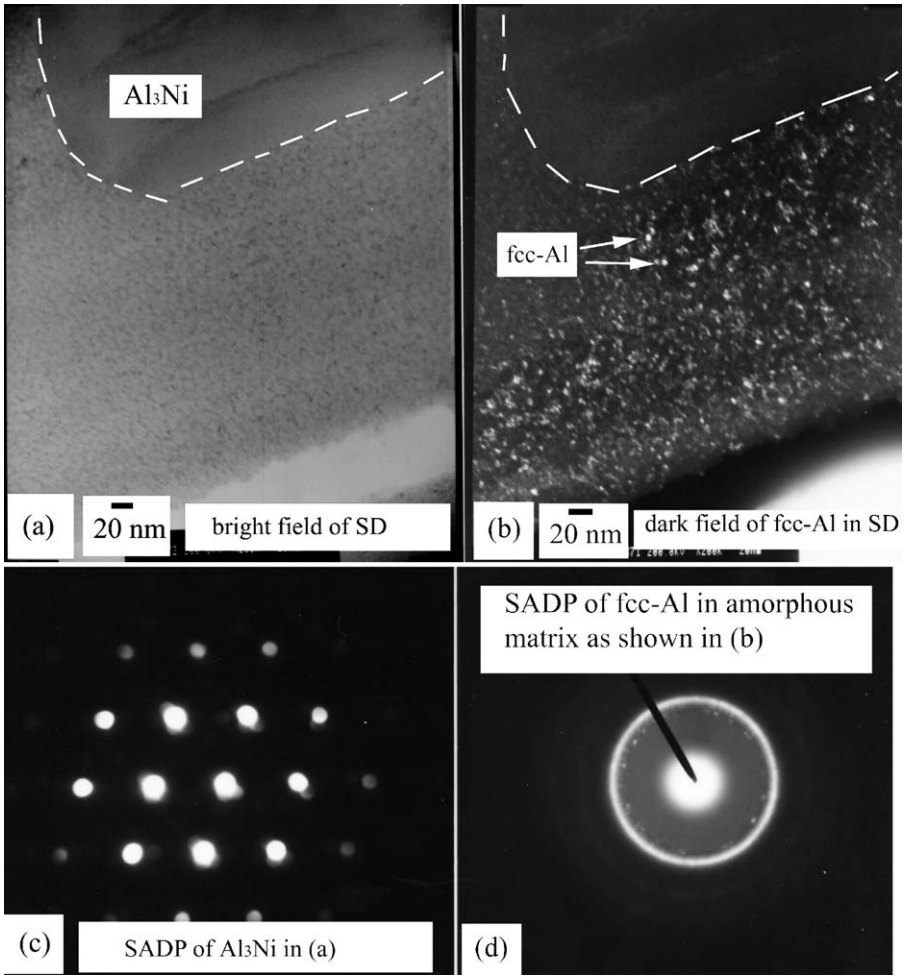

Fig. 6. TEM, micrographs of bright field (a) and dark field (b) images of as-spray-formed deposit (SD). Selected area diffraction patterns (SADP) of rod-like Al_3Ni (primary crystals, 300 nm in width) are shown in (c). Nano-scale fcc-Al (secondary crystal, <5 nm in diameter) exhibiting dotted ring-pattern in (d) dispersed uniformly in the amorphous matrix shown by (b).

study [17]. Metastable $Al_{11}La_3$ phases in the SD contained minor Ni quantities (about 5%) to become $Al_{11}La_3$(Ni), due to the higher solubility of Ni in Al by rapid solidification. The compositions measured by the nano-volume EDS were $75.28 \pm 3\%$ Al, $21.8 \pm 1\%$ La and $5.02 \pm 2\%$ Ni. In addition, some irregular pores were also found in the SD due to incompletely filling of liquid under rapid solidification.

Fig. 5 is the proposed schematic sequence of microstructure evolution during spray forming process. Stage 1 is called amorphous formation during atomization and flight. Large droplets, >20 μm in the $Al_{89}La_6Ni_5$ system, either show precipitation primary crystals in the liquid or become undercooled liquid. Small droplets, <20 μm, either are directly quenched into amorphous solid or become undercooled liquid. Stage 2 is called amorphous formation upon impact on the substrate or free surface of deposit. Upon impacting on the LN-cooled substrate, the undercooled liquid in the large droplets begins to transform into amorphous phase. The top surface layer consists of a mixture of undercooled liquid, liquid, primary crystals, solidified amorphous particles and solidified particles with primary crystals. Stage 3 is called devitrification of amorphous phase during deposition. As the deposit thickens, heat released during solidification reheats the deposit, causing devitrification of amorphous phase and formation of nano-scale secondary fcc-Al crystals (<5 nm). Finally, the deposit is a hybrid composite comprising mixture of amorphous phase, primary crystals and secondary crystals.

Fig. 6 shows bright field (BF) and dark field (DF) images of the SD. In (a) and (b), a large amount of fcc-Al secondary crystals (<5 nm) are shown to disperse uniformly in the amorphous matrix. The dimension of the fcc-Al crystals is close to that of crystals found in annealed melt-spun ribbons. A relatively large rod-like primary Al_3Ni phase (about 300 nm in width) is also observed in Fig. 6, the contour of which is highlight by dotted white lines.

Fig. 7 also corresponds to the BF and DF images of the SD, showing the angular (about 1–2 μm) and round (about 500 nm) primary $Al_{11}La_3$(Ni) phases, containing of many deformation twins, dispersed in the amorphous matrix. During spray forming, stringent temperature gradients, large stirring and impact of droplets during deposition occur, together with misfit of thermal expansion between primary crystals

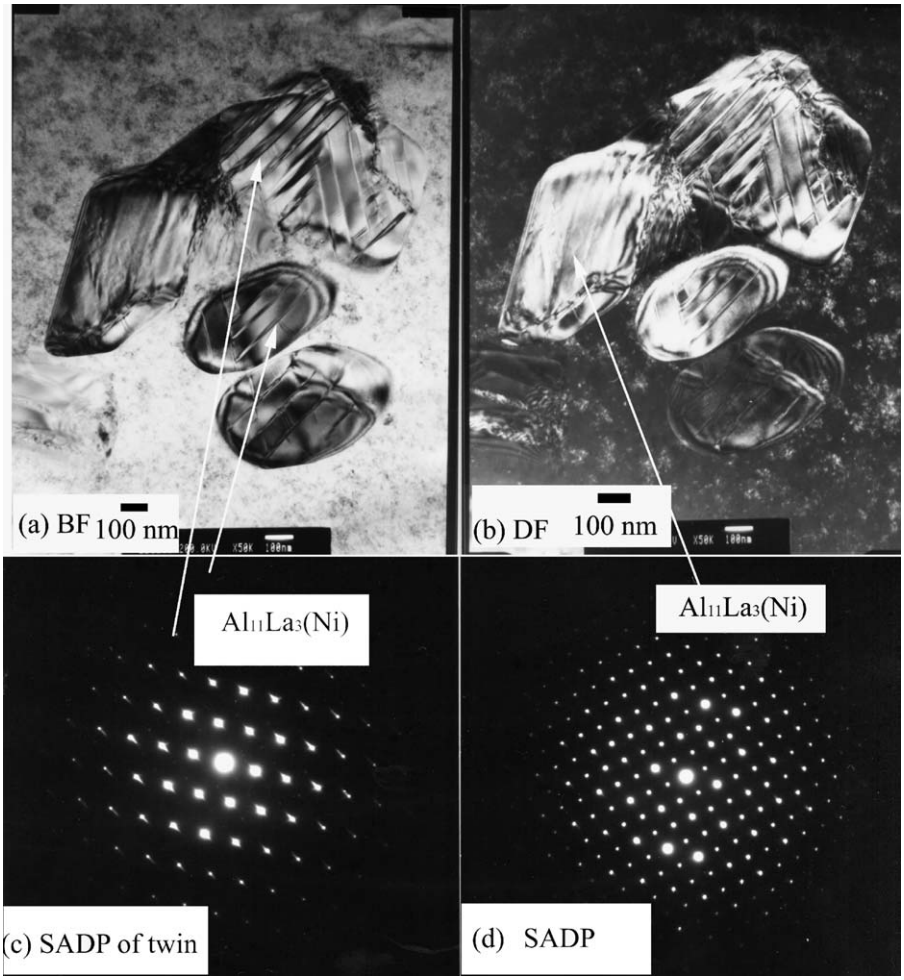

Fig. 7. TEM, micrographs of bright field (a) and dark field (b) images of as-spray-formed deposit (SD). The SADPs of $Al_{11}La_3$(Ni) phase taken on deformation twins and adjacent areas are shown in (c) and (d), respectively.

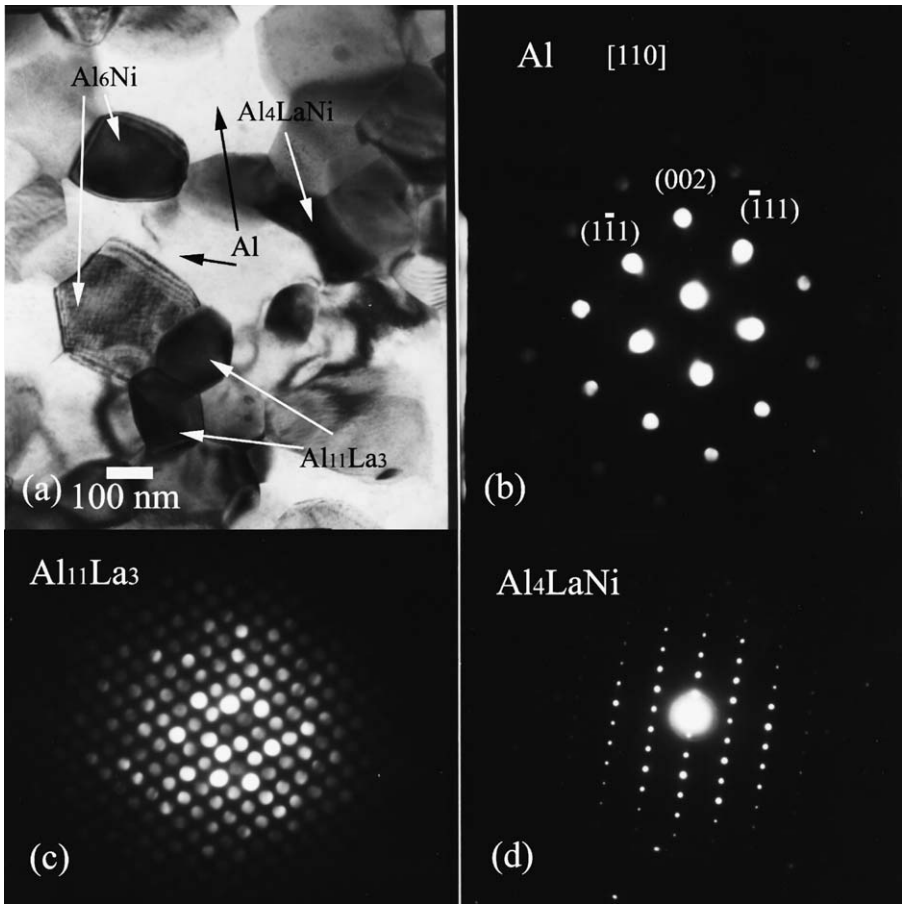

Fig. 8. TEM, micrograph of bright field image of the MS30 (after heated to 823 K) is shown in (a). From (b) to (d) is shown the SADPs of the fcc-Al, $Al_{11}La_3$ and Al_4LaNi crystals taken at the positions arrowed in (a).

and the adjacent amorphous matrix. All of these effects are sufficiently large to trigger deformation twins in the $Al_{11}La_3$(Ni) phase. The SADPs of $Al_{11}La_3$(Ni) phases taken on the deformation twins and adjacent areas are shown in Fig. 7(c) and (d), respectively.

Fig. 8 is a BF image of the fully crystallized MS30 after being heated to 823 K. The heat-treated, fully devitrified microstructure consists of nano-scale Al crystals, binary Al_3Ni, $Al_{11}La_3$, metastable Al_6Ni and ternary Al_4LaNi phases. The grain size of the Al crystals is about 200 nm. No deformation twins are shown in primary crystals, as shown in the SD, which is because the CTE misfit between the nano-scale secondary crystals and the adjacent crystalline matrix was much smaller, so the stress could be eliminated during heat treatment to 823 K.

Therefore, from the XRD, DSC and microanalysis, there are three steps of microstructure evolution during the heating of MS30 to 823 K. The first is the precipitation of fcc-Al crystals in the amorphous matrix, followed by the appearance of Al_3Ni and some amount of metastable Al_6Ni phases. Finally, $Al_{11}La_3$ and ternary Al_4LaNi phases precipitate above 643 K. The grain size is about 200 nm and all the precipitates disperse uniformly. The dimensions of nano-scale secondary crystals, Al_3Ni, Al_6Ni, $Al_{11}La$ and Al_4LaNi, generated in the MS30 during heat-treatment are much smaller than those of the primary crystals, $Al_{11}La_3$(Ni) (about 1–2 μm) and Al_3Ni (about 1 μm) in the SD generated during spray forming.

4. Conclusions

1. The spray-formed $Al_{89}La_6Ni_5$ is a bulk hybrid composite consisting of 36% amorphous phase, and nanostructured phases, including primary crystals of mostly Al_3Ni and $Al_{11}La_3$(Ni) phases, and a large amount of nano-scale Al secondary crystals dispersed uniformly in the amorphous matrix.
2. Melt-spun amorphous ribbons, after being heated to 823 K, become a hybrid composite consisting of binary Al_3Ni, $Al_{11}La_3$ and metastable Al_6Ni and ternary Al_4LaNi phases of the dimension about 200 nm.
3. In the first stage of spray forming, droplets are generated by atomization in the form of completely undercooled liquid, primary crystals in liquid, amorphous solid particles and completely crystallized particles.
4. In the second stage of spray forming, upon droplets impacting on the substrate or free surface of deposit, a semi-solid layer is formed consisting of undercooled

liquid + liquid + primary crystals, solidified particles with primary crystals being deformed upon impacting, solidified amorphous particles being deformed upon impacting, solidified amorphous particles and completely crystallized particles.

5. In the third stage of spray forming, amorphous phase devitrifies to form secondary crystal precipitation and semi-liquid layer solidifies into a mixture of amorphous phase, primary and secondary crystals.
6. Microstructure evolution during devitrification of amorphous melt-spun ribbon upon heating is in three steps: (1) amorphous + fcc-Al; (2) amorphous + fcc-Al + Al_3Ni; (3) Fcc-Al + Al_3Ni + metastable Al_6Ni + $Al_{11}La_3$ + Al_4LaNi.
7. Deformation twins were only observed in the primary $Al_{11}La_3$(Ni) crystals in the spray-formed bulk hybrid composite, but not in the fully devitrified ribbon hybrid composite. The twins were believed to be generated during growth of primary crystals in the amorphous matrix due to large impacts and stirring during spray forming, and thermal expansion coefficient misfit between primary crystal and adjacent amorphous phase.

Acknowledgements

The financial support from the National Science Council and the technical supports of the melt-spun facilities in National Chung Cheng and I-Shou University, the DSC analyzer in China Steel Corporation, and JEOL 3010 TEM in National Sun-Yat-Sen University are kindly acknowledged.

References

[1] G.J. Shiflet, Y. He, S.J. Poon, J. Appl. Phys. 64 (12) (1988) 6863.
[2] L.C. Chen, F. Spaepen, Nature 336 (1988) 366.
[3] A.L. Greer, Science 267 (1994) 1947.
[4] A. Inoue, H. Kimura, J. Light Met. 1 (2001) 31.
[5] J.H. Perepezko, R.J. Hebert, W.S. Tong, Intermetallics 10 (2002) 34.
[6] K. Lu, Mater. Sci. Eng. R 16 (1996) 161.
[7] A. Inoue, Prog. Mater. Sci. 43 (1998) 365.
[8] P.S. Grant, Prog. Mater. Sci. 39 (4–5) (1995) 497.
[9] Y.H. Su, C.-Y.A. Tsao, Metall. Mater. Trans. 28B (12) (1997) 1249.
[10] Y.M. Chen, Y.H. Su, R.W. Lin, C.-Y.A. Tsao, Acta Mater. 46 (3) (1998) 1011.
[11] M.L. Ted Guo, C.Y.A. Tsao, Mater. Sci. Eng. A 326 (1) (2002) 1.
[12] L. Alan, Met. Powder Rep. 54 (5) (1999) 28.
[13] M. Oguchi, A. Inoue, H. Yamaguchi, T. Masumoto, J. Mater. Sci. Lett. 10 (1991) 289.
[14] C.R.M. Afonso, C. Bolfarini, C.S. Kiminami, N.D. Bassim, M.J. Kaufman, M.F. Amateau, T.J. Eden, J.M. Galbraith, Scripta Mater. 44 (2001) 1625.
[15] C.R.M. Afonso, C. Bolfarini, C.S. Kiminami, N.D. Bassim, M.J. Kaufman, M.F. Amateau, T.J. Eden, J.M. Galbraith, J. Non-Cryst. Solid 284 (2001) 134.
[16] A. Inoue, T. Zhang, T. Masumoto, Mater. Trans. JIM 30 (12) (1989) 965.
[17] T. Gödecke, W. Sun, R. Lück, K. Lu, Z. Metallkd. 92 (7) (2001) 717.
[18] F. Ye, K. Lu, Acta Mater. 47 (8) (1999) 2449.
[19] F. Ye, K. Lu, Phys. Rev. B 60 (10) (1999) 7018.
[20] D.V. Louzguine, A. Inoue, J. Non-Cryst. Solid 311 (2002) 281.
[21] D.R. Allen, J.C. Foley, J.H. Perepezko, Acta Mater. 46 (1998) 431.
[22] R.D. Sá Lisboa, C.S. Kiminami, J. Non-Cryst. Solid 304 (2002) 36.
[23] N. Bassim, C.S. Kiminami, M.J. Kaufman, J. Non-Cryst. Solid 273 (2000) 271.